FACTA UNIVERSITATIS
Series: **Physics, Chemistry and Technology** Vol. 3, N° 2, 2005, pp. 95 - 107

EXPLANATION OF THE MEMORY EFFECT IN ARGON

UDC 537.569/.534.8

Vidosav Lj. Marković, Saša R. Gocić, Suzana N. Stamenković

Department of Physics, University of Niš, P.O. BOX 224, 18001 Niš,
Serbia and Montenegro

Abstract. *Memory effect - the long time variation of the electrical breakdown time delay on the relaxation time* $\overline{t_d}(\tau)$, *was observed in argon 24 hours after relaxation times and explained by the long-lived metastable states remaining from the preceding glow. However, the quenching processes reducing the effective lifetime of metastable states several orders of magnitude below that relevant for the time scale of observation were neglected. By applying approximate gas phase models it was found that the early afterglow kinetics up to hundreds of milliseconds is dominated by the decay of molecular argon ions* Ar_2^+ *and the approximate value of their ambipolar diffusion coefficient is determined. After that, nitrogen atoms present as impurities and recombined on the cathode surface and/or field emission determine the breakdown time delay down to the cosmic rays and natural radioactivity level.*

Key words: *electrical breakdown, time delay, memory effect, argon, metastable states.*

1. INTRODUCTION

Investigations of electrical breakdowns and gas discharges were initiated in 1953 in Electronic Industry (Niš) as industrial development of gas-filled tubes, including surge aresters [1-3]. It was found that electrical breakdown time delay t_d depends on different parameters, as well as the afterglow period or relaxation time τ during which there is no voltage on the tube. The dependence of the mean value of at least 100 breakdown time delay data on the afterglow period $\overline{t_d}(\tau)$ was termed memory curve and measured for τ up to 24 hours in gas tubes filled with inert and molecular gases [1-3]. The long-time variation of electrical breakdown time delay on the afterglow period (memory effect) at gas pressures of ~1−100 *mbar* was explained by the action of the hypothetical long lived metastable states remaining from the preceding glow and therefore, the metastable lifetime of 24 hours was assumed. The measurements and metastable hypothesis in argon were repeated recently specifying the $Ar(^3P_0)$ and $Ar(^3P_2)$ metastable states as carriers of the memory effect in argon [4-6], because of their long theoretical radiative lifetimes.

Received May 23, 2005

However, the metastable states are quenched very efficiently by collisions with ground state atoms, electrons, walls and between themselves and even elementary considerations show that their effective lifetimes are very short on the time scale of the observations for the pressures and other conditions of these experiments. The explanation of memory effect in nitrogen based on metastables was shown to be incorrect and a new model was developed in [7-11] based on surface recombination of atoms on the cathode to provide secondary electrons for breakdown initiation. The measurement of breakdown delay was used for atom detection down to cosmic rays and natural radioactivity level and the basic laws of surface collision processes were determined (the mechanism and order of surface recombination, adsorption isotherm, etc.). The explanation and models of memory effect in hydrogen [12,13] based on surface recombination of hydrogen atoms were developed, too.

In a recent paper [14] the memory effect in the flowing technical purity helium was observed. The authors discussed some possible explanations and considered surface recombination of the nitrogen atoms (present as impurities) as the most probable cause of the post-discharge emission. It should also be noted that an afterglow in X_e and K_r with small amounts of nitrogen was observed in [15], and in the case of X_e was followed to ten seconds. The author of this paper proposed nitrogen metastable states and nitrogen atoms as a source of energy storage.

Therefore, in this paper the measurements are carried out in argon in order to test the metastable hypothesis, as well as other mechanisms of secondary electron emission leading to the memory effect. Experimental details related to these experiments are summarized in section 2. In section 3, a simple analytical and more exact numerical gas phase model for metastable and charged particle decay are presented and compared with measurements. In sections 4, the surface recombination of nitrogen atoms and field emission are tested as possible carriers of the memory effect down to the level defined by cosmic rays and natural radioactivity.

2. EXPERIMENTAL DETAILS

The breakdown time delay measurements was performed for a cylindrical-geometry gas tube made of molybdenum glass with volume of $V \approx 300\ cm^3$ and gold-plated copper cathode (copper rods of 99.98% purity and diameter $D = 6\ mm$, inter-electrode distance $d \approx 4.5\ mm$). The tube was evacuated down to $10^{-7}\ mbar$, baked at $600K$, and then filled with argon with an oxygen impurity level below 1 *ppm* (Matheson Co.), at pressure 1.33 *mbar*. The static breakdown voltage was $U_s = 360V$ DC. The time delay measurements were carried out at discharge voltage of $U_w = 540V$, glow currents of $I_g = 0.15mA$, glow time $t_g = 1s$ and relaxation time was varied from milliseconds in the afterglow to the saturation range due to cosmic rays and natural radioactivity.

Before the measurements, the cathode surface was prepared by running a glow discharge for 30 minutes and several hundreds of breakdowns. The mean values of the breakdown delay times were established from series of 100 measurements. During the measurements, the gas tube was protected from light. More details about the experimental procedure and development of measuring system can be found in [7-11]. For these measurements the new electronic system was designed and it is shown in Fig. 1. A personal computer (Pentium IV) with interface was used to control the basic parameters

of the experiment and for acquisition and analysis of data, achieving the resolution limit of 0.18 μs.

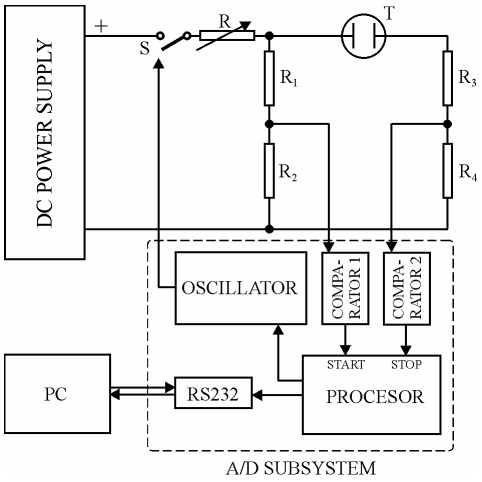

Fig. 1. Electronic system for time delay measurements; R, R_1-R_4 : resistors, T : gas tube, S : electronic switching, PC : personal computer.

3. APPROXIMATE GAS PHASE MODEL OF METASTABLE AND CHARGED PARTICLE DECAY IN EARLY ARGON AFTERGLOW

Analytical solution

Argon has two metastable states $Ar(^3P_2)$ and $Ar(^3P_0)$ with very long radiative lifetimes τ_r of 55.9s and 44.9s, respectively [16]. Since the density of $Ar(^3P_0)$ state is populated by about one order of magnitude lower than the number density of $Ar(^3P_2)$ [17], only the latter metastable state will be followed in the afterglow. The temporal evolution of $Ar(^3P_2)$ metastable state in afterglow in approximate gas phase model [10], is given by equation:

$$\frac{d[Ar^*]}{d\tau} = -(k_{a1}+k_{a2})[Ar^*]^2 - k_e[N_e][Ar^*] - k_2[Ar^*][Ar] - \\ - k_3[Ar^*][Ar]^2 - (D_m/\Lambda^2)[Ar^*] \tag{1}$$

Here, $[Ar^*]$ is the metastable number density and the initial one is estimated to be $[Ar^*] \approx 2\times10^{10} cm^{-3}$ [18]. The k_{a1} and k_{a2} are the rate coefficient for the metastable-metastable collision quenching giving Ar^+ and Ar_2^+ ions, and they are equal $6.3 \times 10^{-10}\ cm^3\ s^{-1}$ and $5.7 \times 10^{-10}\ cm^3\ s^{-1}$, respectively [19]. The k_e is the rate coefficient for quenching in electron collision and it is equal $2 \times 10^{-7}\ cm^3\ s^{-1}$ [20]. We assumed that the number density of electrons $[N_e]$ is approximately equal to the sum of number densities of atomic and molecular ions. Initial number density of atomic ions is estimated from the Poisson equation [10] to be $[Ar^+]_0 \approx 3 \times 10^{10}\ cm^{-3}$ and $[Ar_2^+]_0$ as 1% of atomic ions number density [21]. The $k_2 = 2.1 \times 10^{-15}\ cm^3\ s^{-1}$ is the rate coefficient for two-body

quenching in collisions with ground-state atom [17] and $k_3 = 1.1 \times 10^{-32}\ cm^6\ s^{-1}$ for three-body quenching in collisions with two ground state atoms [17]. The last term of (1) describes diffusion, followed by quenching on the walls with unit probability. The diffusion time constant τ_d can be expressed by $1 / \tau_d = D_m / \Lambda^2$, where $D_m = 54.9\ cm^2\ s^{-1}$ is the diffusion coefficient of $Ar(^3P_2)$ metastable state in the parent gas [17] and $\Lambda \approx 1.1\ cm$ is the characteristic diffusion length of the tube. Radiative deexcitation is negligible because the radiative lifetime is very long [16].

With these assumptions, the analytical solution of equation (1) is:

$$[Ar^*] = \frac{[Ar^*]_0 \exp(-\nu_s \tau)}{1 + [(k_{a1} + k_{a2}) / \nu_s][Ar^*]_0 [1 - \exp(-\nu_s \tau)]} \tag{2}$$

where the total loss frequency $\nu_s = k_e [Ar^*] + k_2 [Ar] + k_3 [Ar]^2 + D_m / \Lambda^2$ includes the first order loss processes. The second order process of metastable-metastable collision quenching in the very early afterglow has the loss frequency of 24 s^{-1}, which is negligible compared to the electron quenching with the loss frequency of 6000 s^{-1}. Because the electron and metastable number densities decay very quickly within the first several milliseconds for which we do not have the experimental data, our further discussion will rely on the other first order processes acting all the time in the afterglow and depending only on the pressure of the parent gas. Even if we neglect the electron quenching, the first order processes are predominant $\nu_s >> (k_{a1} + k_{a2})\,[Ar^*]$ after several milliseconds in afterglow and the exponential temporal evolution of metastable states is obtained:

$$[Ar^*] = [Ar^*]_0\, e^{-\nu_s \tau} \tag{3}$$

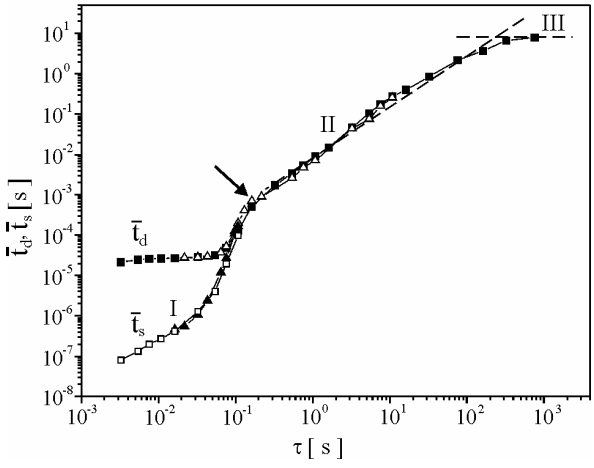

Fig. 2. Memory curves in argon (■ - $\bar{t}_d$ and □ - $\bar{t}_s$ of basic measurements, Δ - $\bar{t}_d$ and ▲ - $\bar{t}_s$ refer to repeated measurements after 24 hours).

Now, we will try to fit the experimental breakdown time delay data (Fig. 2, region I) on the basis of relation (3). It is well known that the total time delay comprises the statistical time delay t_s and the formative time t_f, i.e. $t_d = t_s + t_f$ [22]. The statistical time delay can be expressed as [22]:

$$\bar{t}_s = 1/YP \tag{4}$$

where Y - represents a number of generated electrons in the inter-electrode space per second (electron yield), and P - is the probability of one electron to cause the breakdown. In our conditions, P ≈ 0.8 is determined in the same way as described in [7]. The standard deviation of the statistical time delay is $\sigma = \bar{t}_s$ [23] and the statistical time delay $\bar{t}_s(\tau)$ is used to follow the afterglow kinetics in region I (Figs. 2, 3). In the regions II and III, the formative time t_f can be neglected [10] and relation $\bar{t}_d \approx 1/YP$ is used to study late afterglow kinetics.

If the breakdown time delay in the region I of the memory curve is caused by metastable induced secondary electron emission then:

$$Y = \gamma_m \frac{[Ar^*]\,\bar{v}_m}{4} S_c \tag{5}$$

where γ_m is the secondary electron yield caused by metastable collision, $\bar{v}_m = 3.9\times10^4\ cm\,s^{-1}$ is the mean thermal velocity and $S_c = 0.28\ cm^2$ the front area of the cathode surface. By combining the equations (3), (4) and (5), the value of the v_s can be obtained in the form:

$$[Ar^*] = [Ar^*]_0\, e^{-\nu_s \tau} \tag{6}$$

or, inversely the effective lifetime $\tau_{eff} = 1 / \nu_s$. The $t_{s\,0}$ is the corresponding value at $\tau = 0$ in the afterglow. Thus, if $\bar{t}_s(\tau)$ for the region I is presented in the semi-log scale, the dependence is linear confirming the assumed first order decay in this afterglow period (Fig. 3), and from relation (6) it follows that $\nu_s \approx 62.2\ s^{-1}$, or the effective lifetime $\tau_{eff} \approx 16.1\ ms$.

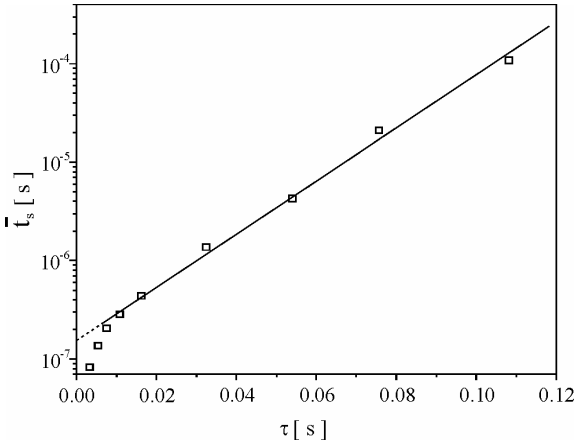

Fig. 3. Memory curve for the region *I* (□) and least-square fit (solid line).

A review of the measurements of diffusion and rate coefficients found in the literature for the most important first order processes are presented in Table 1. The diffusion coefficients refer to 1.33*mbar* and are normalized to the room temperature of 293 *K*. The total loss frequency in all cases is calculated and shown in the last column. Thus, the total loss frequency varies in the range (95 – 153) s^{-1}, and can be used for comparison with our experimental data (Fig. 3). For the coefficients cited in Table 1, loss frequency is greater by about 1.5 – 2.5 times than the experimentally obtained value, even though some even faster quenching processes effective in early phases of the afterglow were neglected in the model. The effective lifetimes exceed by far the uncertainty of the well-established data and thus we may conclude that the afterglow is not dominated by metastables.

At higher pressures a discrepancy between estimated metastable lifetimes in [1-6] and our calculations is even drastic. For example, the memory effect in argon has been observed even at the pressures of 40 *mbar* [2] and 66.5 *mbar* [4]. Under those conditions and even if we use the smallest coefficients and loss frequency from the measurements in [26], the loss frequency at 66.5 *mbar* is $\nu_s \sim 37000\, s^{-1}$, or the effective lifetime $\tau_{eff} \sim 27\ \mu s$, showing that metastable hypothesis completely failed to explain the memory effect in argon lasting of minutes or even hours.

Table 1. The diffusion and rate coefficients, accompanied by the loss frequencies for the important first order processes.

$D_m[\frac{cm^2}{s}]$	$k_2[10^{-15}\frac{cm^3}{s}]$	$k_3[10^{-32}\frac{cm^6}{s}]$	$\nu_s\left[\frac{1}{s}\right]$	References
54.9	2.1	1.1	127.8	[17]
51.0	1.0	1.7	94.7	[24]
53.0	1.2	0.85	94.7	[25]
47.0	1.2	1.3	93.7	[26]
50.0	1.36	1.65	105.2	[27]
39.9	1.85	2.9	126.3	[28]
44.1	2.8	1.9	150.4	[29]
72.8	2.3	1.4	152.9	[30]

According to our calculations within the first milliseconds of the afterglow, atomic ion Ar^+ is dominant, but after that the molecular ions Ar_2^+ begin to dominate due to atomic-molecular ion conversion in collisions with two ground state atoms. The rate coefficient for this process is $k_c = 2.26 \times 10^{-31}\ cm^6\ s^{-1}$ [31]. The diffusion time constant τ_i for our cylindrical geometry, assuming that the zero of the fundamental mode coincides with the container walls, is given by $1 / \tau_i = D_{a2} / \Lambda^2$, where D_{a2} is the ambipolar diffusion coefficient of molecular argon ions. By using foregoing relation with $\tau_i = \tau_{eff} \approx 16.1\ ms$, it follows that $D_{a2} \approx 73\ cm^2\ s^{-1}$. This value is in good agreement with experimental data from [31, 32] where $D_{a2} = 69.2\ cm^2\ s^{-1}$ is obtained. In the subsequent section we will apply a numerical solution of coupled differential equations by including all the relevant processes of metastable and charged particle kinetics in argon afterglow.

Numerical solution

The temporal evolution of the $Ar(^3P_2)$ metastable state and Ar^+ and Ar_2^+ ions can be followed by numerically solving the system of ordinary differential equations (7-9) and for the electron yield in the inter-electrode space (10):

$$\frac{\partial[Ar^*]}{\partial\tau} = -(k_{a1}+k_{a2})[Ar^*]^2 - k_e[N_e][Ar^*] - k_2[Ar^*][Ar] - k_3[Ar^*][Ar]^2 - (D_m/\Lambda^2)[Ar^*] + k_r[Ar_2^+][N_e] \tag{7}$$

$$\frac{\partial[Ar^+]}{\partial\tau} = k_{a1}[Ar^*]^2 - k_c[Ar^+][Ar]^2 - (D_{a1}/\Lambda^2)[Ar^+] \tag{8}$$

$$\frac{\partial[Ar_2^+]}{\partial\tau} = k_{a2}[Ar^*]^2 + k_c[Ar^+][Ar]^2 - k_r[Ar_2^+][N_e] - (D_{a2}/\Lambda^2)[Ar_2^+] \tag{9}$$

$$Y = C\cdot\{\gamma_m[Ar^*]\,\bar{v}_m/4 + \gamma_{i1}[Ar^+]\,\bar{v}_{i1}/4 + \gamma_{i1}[Ar^+]\,w_{i1} + \gamma_{i2}[Ar_2^+]\,\bar{v}_{i2}/4 + \gamma_{i2}[Ar_2^+]\,w_{i2}\}\,S_c \tag{10}$$

where C is the proportionality constant, including the factors related to electrode geometry, electron distributions, etc. For the electron-ion dissociative recombination giving one metastable state, the value of rate coefficient $k_r = 8.5\times10^{-7}\ cm^3\,s^{-1}$ was used [33], where $[N_e] = [Ar^+] + [Ar_2^+]$. The electron- Ar^+ radiative recombination (rate coefficient $\sim10^{-11}\ cm^3\,s^{-1}$ [34]) is negligible under our conditions. Second terms in equations (8,9) represent the atomic-molecular conversion and third – diffusion followed by electron-ion recombination on the walls. The values used in our model for the ambipolar diffusion coefficients are $D_{a1} \approx 71\ cm^2\,s^{-1}$ and $D_{a2} \approx 69.2\ cm^2\,s^{-1}$, for the atomic and molecular ions, respectively [31,32]. The γ_{i1} and γ_{i2} are the secondary electron yields caused by Ar^+ and Ar_2^+ ions, respectively, and $\bar{v}_{i1} = 3.9\times10^4\ cm\,s^{-1}$ and $\bar{v}_{i2} = 2.4\times10^4\ cm\,s^{-1}$ are their mean thermal velocities. Also, the $w_{i1} = 3\times10^5\ cm\,s^{-1}$ and $w_{i2} = 4.5\times10^5\ cm\,s^{-1}$ are their drift velocities to the cathode after the application of voltage, respectively, estimated from [35]. System of equations (7-10), representing the gas phase model of afterglow kinetics in argon is solved by using fourth-order Runge-Kutta method. The fitting parameters are adjusted in order to fit the experimental data. Best fit of experimental data (Fig. 4) is obtained for $C\gamma_m = 9.5\times10^{-8}$, $C\gamma_{i1} = 9.8\times10^{-9}$ and $C\gamma_{i2} = 1.6\times10^{-7}$. The fitting parameters in this model give only apparent secondary electron yields due to neglect of number density space profiles, whose calculations are carried out in diffusive model [36]. With our models, it is shown that only the decay of molecular argon ions Ar_2^+ can fit experimental values for the electron yield versus τ and explain the early memory effect in argon (Fig. 4). The metastable states have a very fast decrease and cannot fit the slope of experimental data (Fig. 4, dotted line). It should be noted that no variation in the initial density of metastables would give a good fit over the whole afterglow period since slopes would be quite different. If we reduce the assumed metastable densities it will only increase the secondary electron yield, and vice versa.

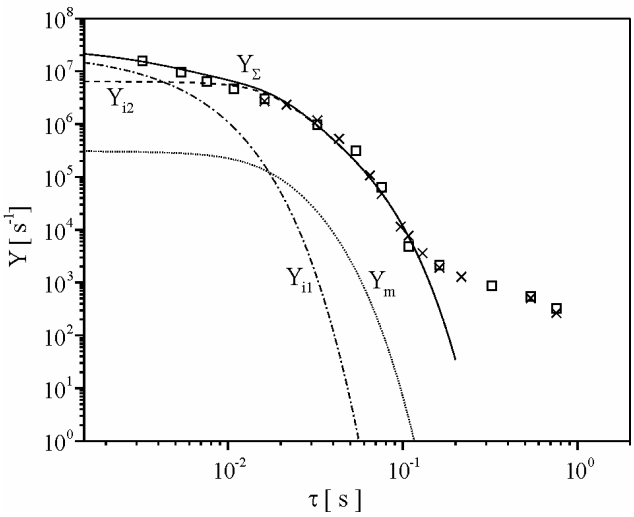

Fig. 4. Total electron yield Y_Σ in the region I (solid line), with contributions from molecular ions Y_{i2} (dashed line), atomic ions Y_{i1} (dash-dot line) and from metastable states (dotted line).

4. EXPLANATION OF LATE MEMORY EFFECT

Gas phase model of surface recombination of nitrogen atoms

The metastable hypothesis completely failed to explain memory effect and now we will test the surface recombination of nitrogen atoms present as impurities, as proposed in [14] for helium. The effect of the surface-catalyzed excitation was observed in [37-40], when it was discovered that electronically excited molecules of nitrogen could be formed by recombination of *N* atoms on certain metal surfaces. Spectroscopic and photographic analysis indicates formation of $N_2(A^3\Sigma_u^+)$ metastables on the metal surface, which diffuse into the gas phase and are converted into the $N_2(B^3\Pi_g)$, which radiates giving the first positive system of nitrogen molecule [37-40].

Now the surface recombination hypothesis in argon will be tested by applying the gas phase model of afterglow kinetics of nitrogen atoms. More details about this model, as well as comparison with the diffusive model, can be found in [36,41]. The main loss processes of nitrogen atoms in the afterglow are the recombination on the glass walls and the surface recombination of atoms on electrodes, with or without forming excited molecules, are responsible for production of secondary electrons and initiation of breakdown [7]. In the homogeneous gas phase representation of surface losses, the loss rates of the density of nitrogen atoms during the afterglow and the electron yields are given by equations [9,41]:

$$\frac{d[N]}{d\tau} = -\gamma_{mw}[N]^2 \tag{11}$$

$$Y = \gamma_1 [N] V_C + \gamma_2 [N]^2 V_C + Y_0 \tag{12}$$

where γ_{nw} designates the effective gas phase rate coefficient for the second order surface recombination on glass walls, V_c is the volume of the inter-electrode space, Y_0 is the "background" electron yield and γ_1, γ_2 are the effective gas phase rate coefficients for the surface recombination on the cathode and are first and second order, respectively. These rate coefficients in (11) and (12) are defined in relation to the gas-phase number density of nitrogen atoms [7,9,41]. The plateau of the saturation region III (Fig. 2) is determined by the cosmic rays and natural radioactivity level and is used to determine "background" electron yield as $Y_0 \approx 1/(\overline{t_d^{sat}}\, P) \approx 0.1 s^{-1}$.

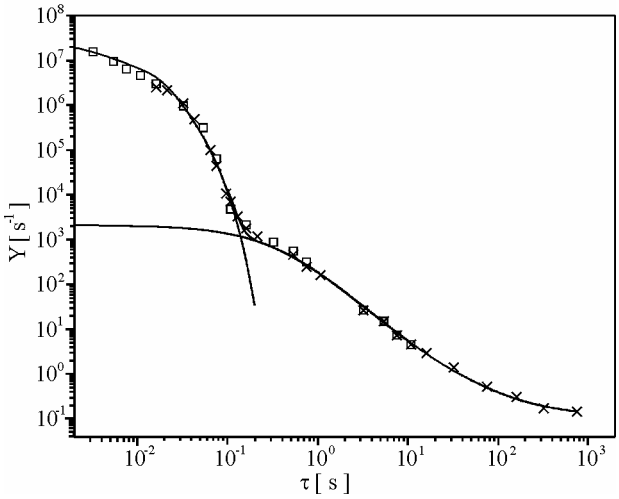

Fig. 5. Fitting of the memory curve in the late afterglow based on surface recombination of nitrogen atoms (the right solid line).

The initial number density of nitrogen atoms is assumed to be $[N]_0 = 3.3 \times 10^9\ cm^{-3}$ which corresponds to about 1 *ppm* impurity content of nitrogen in argon and degree of dissociation of ~10%. Degree of dissociation was found to increase when the fraction of nitrogen in argon decreases [42,43], and typical value is of the order of 10%. One may argue that contamination may increase by outgassing of the walls and during the sealing procedure but even for 1 *ppm* we can fit the experimental data with realistic degree of dissociation. The best fit for the region II of the memory curve is obtained for $\gamma_{nw} = 7.5 \times 10^{-10}\ cm^3\ s^{-1}$, $\gamma_1 = 1.2 \times 10^{-7}\ s^{-1}$ and $\gamma_2 = 1.2 \times 10^{-15}\ cm^3\ s^{-1}$ (Fig. 5, the right solid line). The coefficients γ_1 and γ_2 include the probability of secondary electron emission through the adsorbed layer of argon atoms. As for the estimation of the initial nitrogen atom number density in the afterglow, the conjugation relation also holds $\gamma_{nw}[N_0] = const$, which means that if $[N_0]$ increases, then γ_{nw} decreases, and vice versa. Support of this thesis is the observation of afterglow in X_e and K_r with a small amount of nitrogen. The afterglow was followed to ten seconds in X_e [15] and the author proposed nitrogen metastable states and nitrogen atoms as a source of energy storage.

Influence of field emission

Now we will test the field emission for the explanation of the memory effect as proposed in [44] for SF_6. According to Fowler-Nordheim formula [45], dependence of the field emission current I on the voltage U can be expressed by:

$$I = A_{\exp} U^2 \exp\left(-\frac{B_{\exp}}{U}\right) \tag{13}$$

where $B_{\exp}$ is the experimental values of the slope and $A_{\exp}$ the intersection with the ordinate axis, when $\ln(I / U^2)$ is plotted versus $1 / U$. In our case, field emission current is proportional to $I \infty YP$, where P acts as an attenuation factor (except when it is unity) and should be determined and eliminated. The breakdown probability is fitted by a procedure similar to that for determination of breakdown probability [46]. The breakdown probability for the Townsend breakdown mechanism is used, given by relation [47]:

$$P = \begin{cases} 0, & for \quad q < 1 \\ 1 - 1/q & for \quad q > 1 \end{cases} \tag{14}$$

where $q = \gamma_{eff}\ [\exp(\alpha d) - 1]$ and γ_{eff} increases from $0.014 - 0.084$. The data for the dependence of electron ionization coefficient on the reduced electric field $\alpha / N\,(E / N)$ was used from [48].

In our case for untreated cathode $YP(U)$ dependence does not reach saturation at high voltages, but continuously increases (or inversely $\overline{t_d}(U)$ dependence measured at $\tau = 1s$ continuously decreases). Since breakdown probability tends to unity at high voltages ($P \to 1$), it follows that Y should rise in order to fit experimental data, which was confirmed by the Fowler-Nordheim plot for field emission (Fig. 6). The slope of the Fowler-Nordheim plot changes, showing the high field emission for untreated cathode

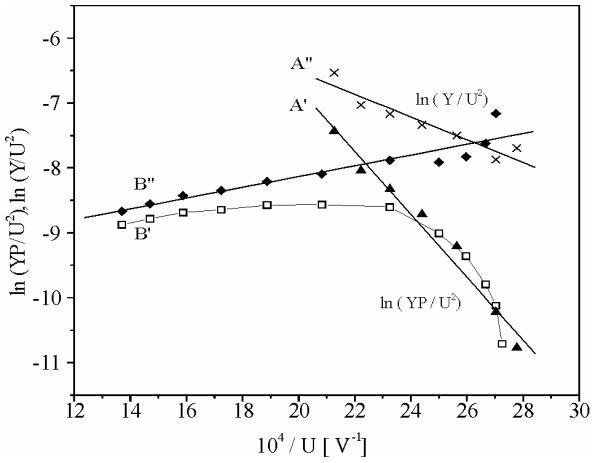

Fig. 6. Test on field emission based on the Fowler-Nordheim plot obtained from $\overline{t_d}(U)$ dependence at $\tau = 1s$ for untreated (curves A' and A") and treated cathode (curves B' and B").

(curve A' with *P* and A" without *P*) and very low field emission for thoroughly treated cathode by several days of glowing and tens thousands breakdowns (curve B' with *P* and B" without *P*). Other measurements from the literature are analyzed and a high field emission was observed. Results of our analysis are shown in Fig. 7, curves C' and C" for measurements in [4], and curves D and E for measurements in [2]. In the case of [2], the situation is simpler, because the discharge voltage was very high and the breakdown probability is close to unity (Fig. 7, curves D and E). The authors of [44] explained memory effect in SF_6 by chemical effects and development of surface layers.

In the case of iron and copper cathode in argon [2,4], the observed field emission may be due to surface charges on an oxide insulating layer or impure cathode (Paetow-Malter effect) [49,50]. The iron oxide was actually confirmed by EDS analysis [51] for iron electrode. Even for gold plated electrodes one may expect a thin oxide coating on the surface [52,53]. The presence of contaminating films and microroughness, as well as negative ions and electronegative molecules on them, could also be a source of electrons initiating breakdown [23,54,55]. The surface migration of metal atoms or clusters [56] can cause the field emission, too.

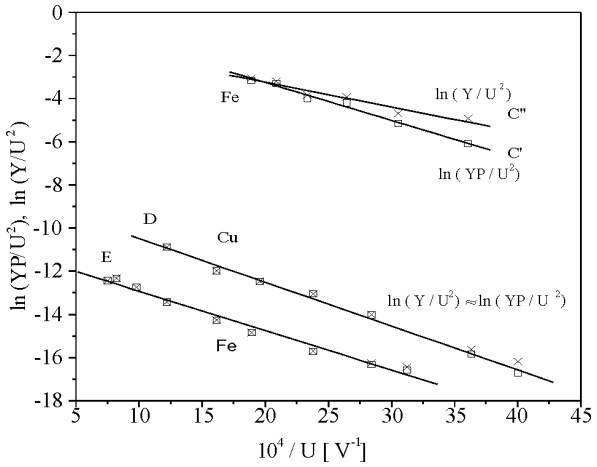

Fig. 7. Test on field emission based on the Fowler-Nordheim plot for the measurements of [4] (curves C' and C") and [2] (curves D and E).

One should argue, however, that the oxide layer may increase the probability of secondary electron emission only if there are charges accumulated on the surface. The time dependence may arise from the long-term surface diffusion of charges on dielectric surface which was shown to have characteristic lifetime of the order of several hours before surface charges are recombined and field disappears [57]. Although there is a possibility that field emission made a contribution in some experiments, its time dependence would be more difficult to model for quantitative comparison in the same way as atom recombination.

5. CONCLUSION

Memory effect in argon [1-6] was explained by the action of long-lived metastable states remaining from the preceding glow. However, these authors have neglected the well known quenching processes which reduce the effective lifetime of metastable states down to the order of milli- and microseconds for their experimental conditions. In this paper the measurements are carried out and approximate and more exact numerical gas phase models are developed in order to study afterglow kinetics in the same range of experimental conditions. It was found that the metastable hypothesis completely failed to explain the memory effect in argon, but charged particle decay can explain the afterglow kinetics to hundreds of milliseconds. For longer afterglow times the surface recombination of nitrogen atoms present as impurities and/or field emission are able to explain the memory effect in argon down to the level determined by cosmic rays and natural radioactivity. It was shown that the experimental technique of following the breakdown delay times can be used to follow the decay of ions and neutral active species and quantitative explanation of the memory effect was given from very short to very long afterglow times

Acknowledgments. *Authors are grateful to Ministry of Science and Environmental Protection of Serbia for partial support (project 1478) and dr Z. Lj. Petrović for useful discussion.*

REFERENCES

1. Dj. A. Bošan, Industrial R and D Report TD-PO2 (Comp. Elektronska industrija, former: Zavodi RR, Niš) 1956
2. Dj. A. Bošan, *Proc. 5th Int. Conf. on Gas Discharges* (Liverpool, UK) *(Stevenage: IEEE)* (1978) 273
3. Dj. A. Bošan, *Invited Lecture at 16th Symposium on the Physics of Ionized Gases* (Belgrade, Yugoslavia) (1993) 171, (ed. M. Milosavljević and Z. Petrović, Nova Science Publishers) (1996) 15
4. M. M. Pejović and G. S. Ristić, *Phys. Plasmas* **9** (2002) 364
5. M. M. Pejović, G. S. Ristić and J. P. Karamarković, *J. Phys. D: Appl. Phys*. **35** (2002) R91
6. M. M. Pejović, G. S. Ristić and J. P. Karamarković, *Facta Universitatis, Series: Physics, Chemistry and Technology* **2** (2000) 63
7. V. Lj. Marković, Z. Lj. Petrović and M. M. Pejović, *J. Chem. Phys*. **100** (1994) 8514
8. V. Lj. Marković, M. M. Pejović and Z. Lj. Petrović, *J. Phys. D: Appl. Phys*. **27** (1994) 979
9. V. Lj. Marković, M. M. Pejović and Z. Lj. Petrović, *Plasma. Chem. Plasma Process.* **16** (1996) 195
10. V. Lj. Marković, Z. Lj. Petrović and M. M. Pejović, *Plasma Sources Sci. Technol.* **6** (1997) 240
11. Z. Lj. Petrović, V. Lj. Marković, M. M. Pejović and S. R. Gocić, *J. Phys. D: Appl. Phys.* 34 (2001) 1756
12. V. Lj. Marković, M. M. Pejović and Z. Lj. Petrović, *Proc. 13-th ESCAMPIG* (Poprad, Slovakia) Vol. **20E**, Part A (1996) 45
13. V. Lj. Marković, M. M. Pejović, Z. Lj. Petrović and S. S. Manola, *Balkan Physics Letters* **5** (1997) 133
14. V. Kudrle, E. LeDuc and M. Fitaire, *J. Phys. D: Appl. Phys*. **32** (1999) 2049
15. C. Kenty, *J. Chem. Phys.* **47** (1967) 2545
16. N. E. Small-Warren and L. Y. Chin, *Phys. Rev.* **A11** (1975) 1777
17. J. H. Kolts and D. W. Setser, *J. Chem. Phys.* **68** (1978) 1978
18. C. M. Ferreira and A. Ricard, *J. Appl. Phys.* **54** (1983) 2261
19. N. B. Kolokolov and A. B. Blagoev, *Phys. Usp.* **36** (1993) 152
20. D. P. Lymberopoulos and D. J. Economou, *J. Phys. D: Appl. Phys.* **73** (1993) 3668
21. A. Bogaerts and R. Gijbels, *J. Appl. Phys*. **86** (1999) 4124
22. C.G. Morgan, *Irradiation and Time Lag, in Electrical Breakdown of Gases* edited by J. M. Meek and J. D. Craggs, John Wiley&Sons, Chichester, 1978
23. F. Llewellyn-Jones and E. T. de la Perrelle, *Proc. Roy. Soc. A* **216** (1953) 267
24. E. Ellis and N. D. Twiddy, *J. Phys. B* **2** (1969) 1366
25. A. V. Phelps and J. P. Molnar, *Phys. Rev.* **89** (1953) 1202

26. A. H. Futch and F. A. Grant, *Phys. Rev.* **104** (1956) 356
27. W. Wieme and J. Wieme-Lenaerts, *Phys. Lett*. **47A** (1974) 37
28. N. Sadeghi-Kharrazi, *Ph.D Thesis,* Grenoble*,* (1974)
29. A. A. Tabačnik, S. J. Umanski and B. R. Šub, *Himičeska fizika* ***7*** (1983) 938 (in Russian)
30. H. Tachibana, *Phys. Rev. A* **34** (1986) 1007
31. M. Sugawara, T. Okada and Y. Kobayashi, *J. Phys. D: Appl. Phys.* **19** (1986) 1213
32. T. Okada and M. Sugawara, *J. Phys. D: Appl. Phys.* **26** (1993) 1680
33. F. J. Mehr and M. A. Biondi, *Phys. Rev.* **176** (1968) 322
34. M. A. Biondi, *Phys. Rev.* **129** (1963) 1181
35. A. von Engel, *Electric Plasmas: Their Nature and Uses,* Taylor&Francis Ltd, London and New York, 1983
36. V. Lj. Marković, S. R. Gocić, S. N. Stamenković and Z. Lj. Petrović, submitted to Physics of Plasmas
37. R. R. Reeves, G. G. Manella and P. Harteck, *J. Chem. Phys.* **32** (1960) 946
38. G. G. Mannella and P. Harteck, *J. Chem. Phys*. **34** (1961) 2177
39. G. G. Mannella, R. R. Reeves and P. Harteck, *J. Chem. Phys.* **33** (1960) 636
40. P. Harteck, R. R. Reeves and G. G. Manella, *Can. J. Chem.* **38** (1960) 1648
41. V. Lj. Marković, Z. Lj. Petrović and M. M. Pejović, *J. Phys. III France* **6** (1996) 959
42. P. A. Sa and J. Loureiro, *J. Phys. D: Appl. Phys*. **30** (1997) 2320
43. A. Ricard, A. Besner, J. Hubert and M. Moisan, *J. Phys. B: At. Mol. Opt. Phys.* **21** (1988) L579
44. G. A. Woolsey and D. B. Ogle, *J. Appl. Phys.* **66** (1989) 2920
45. R. H. Fowler and L. Nordheim, *Proc. R. Soc. A* **119** (1928) 173
46. V. Lj. Marković, S. R. Gocić, S. N. Stamenković, Z. Lj. Petrović and M. Radmilović, *Eur. Phys. J. AP* **14** (2001) 171
47. R. A. Wijsman, *Phys. Rev.* **75** (1949) 833
48. A. V. Phelps and Z. Lj. Petrović, *Plasma Sources Sci. Technol.* **8** (1999) R21
49. H. Paetow, *Z. Phys.* **111** (1939) 770
50. L. Malter, *Phys. Rev.* **50** (1936) 48
51. M. M. Pejović, G. S. Ristić and Z. Lj. Petrović, *J. Phys. D: Appl. Phys.* **32** (1999) 1489
52. Z. Lj. Petrović and A. V. Phelps, *Phys. Rev. E* **47** (1983) 2806
53. Z. Lj. Petrović and A. V. Phelps, *Phys. Rev. E* **56** (1997) 5920
54. F. Llewellyn - Jones and C. G. Morgan, *Proc. Roy. Soc. A* **218** (1953) 88
55. C. G. Morgan and D. Harcombe, *Proc. Phys. Soc. B* **66** (1953) 665
56. B. Jütner, *J. Phys. D: Appl. Phys.* **32** (1999) 2544
57. Z. Lj. Petrović, *PhD thesis,* Australian National University (1985).

OBJAŠNJENJE MEMORIJSKOG EFEKTA U ARGONU

V. Lj. Marković, S. R. Gocić, S. N. Stamenković

Memorijski efekat tj. zavisnost srednje vrednosti vremena kašnjenja električnog proboja u funkciji vremena relaksacije $\overline{t_d}(\tau)$*, je primećen u argonu i do 24 časa nakon prekida pražnjenja i objašnjen je dejstvom metastabilnih stanja zaostalih iz prethodnog pražnjenja. Međutim, pri tome je zanemareno sudarno gašenje metastabilnih stanja što njihovo efektivno vreme života redukuje do nivoa reda mili- i mikrosekundi u datim eksperimentalnim uslovima. U ovom radu je pokazano na osnovu aproksimativnih gasno-faznih modela da je rani memorijski efekat do stotinu milisekundi nakon prekida ražnjenja određen raspadom molekulskih jona argona* Ar_2^+ *i određena je približna vrednost njihovog koeficijenta ambipolarne difuzije. Nakon toga, rekombinacija atoma azota (prisutnih kao nečistoće) na površini katode i/ili emisija poljem određuju vreme kašnjenja proboja sve do nivoa kosmičkog zračenja i prirodne radioaktivnosti okoline.*